arXiv:1612.02067v1 [cs.SY] 6 Dec 2016

Collaborative Visual Area Coverage[☆]

Sotiris Papatheodorou, Anthony Tzes, Yiannis Stergiopoulos[1]

Abstract

This article examines the problem of visual area coverage by a network of Mobile Aerial Agents (MAAs). Each MAA is assumed to be equipped with a downwards facing camera with a conical field of view which covers all points within a circle on the ground. The diameter of that circle is proportional to the altitude of the MAA, whereas the quality of the covered area decreases with the altitude. A distributed control law that maximizes a joint coverage-quality criterion by adjusting the MAAs' spatial coordinates is developed. The effectiveness of the proposed control scheme is evaluated through simulation studies.

Keywords: Cooperative Control, Autonomous Systems, Area Coverage, Robotic Camera Networks

1. Introduction

Area coverage over a planar region by ground agents has been studied extensively when the sensing patterns of the agents are circular [1, 2]. Most of these techniques are based on a Voronoi or similar partitioning [3, 4, 5] of the region of interest and use distributed optimization, model predictive control [6, 7] or game theory [8] among other techniques. There is also significant work concerning arbitrary sensing patterns [9, 10, 11] avoiding the usage of Voronoi partitioning [12, 13]. Both convex and non-convex domains have been examined [14, 15].

[☆]This work has received funding from the European Union's Horizon 2020 Research and Innovation Programme under the Grant Agreement No.644128, AEROWORKS. A shorter version, without the stability–notion and subsequent proof has been submitted for possible inclusion at the ICRA 2017 proceedings.

[1]The authors are with the Electrical & Computer Engineering Department, University of Patras, Rio, Achaia 26500, Greece. Corresponding author's email: tzes@ece.upatras.gr

Many algorithms have been developed for mapping by MAAs [16, 17, 18, 19] relying mostly in Voronoi-based tessellations or path–planning. Extensive work has also been done in area monitoring by MAAs equipped with cameras [20, 21]. In these pioneering research efforts, there is no maximum allowable height that can be reached by the MAAs and the case where there is overlapping of their covered areas is considered an advantage as opposed to the same area viewed by a single camera. There are also studies on the connectivity and energy consumption of MAA networks [22, 23].

In this paper the persistent coverage problem of a convex planar region by a network of MAAs is considered. The MAAs are assumed to have downwards facing visual sensors with a conical field of view, thus creating a circular sensing footprint. The covered area as well as the coverage quality of that area are dependent on the altitude of each MAA. MAAs at higher altitudes cover more area but the coverage quality is smaller compared to MAAs at lower altitudes. A partitioning scheme of the sensed region, similar to [12], is employed and a gradient based control law is developed. This control law leads the network to a locally optimal configuration with respect to a combined coverage-quality criterion, while also guaranteeing that the MAAs remain within a desired range of altitudes. The main contribution of this work is the guarantee it offers that all MAAs will remain within a predefined altitude range. In addition to that, overlapping between the sensed regions of different MAAs is avoided if possible, in contrast to previous works which consider it an advantage.

The problem statement and the joint coverage–quality criterion are presented in Section 2. The chosen quality function is defined in Section 3 and the resulting sensed space partitioning scheme in Section 4. The distributed control law is derived and its most notable properties explained in Section 5. The stability of the altitude control law and its property to restrict the nodes' altitude is examined in Section 6. Simulation studies highlighting the efficiency of the proposed control law are provided in Section 7 followed by concluding remarks.

2. Problem Statement

Let $\Omega \subset \mathbb{R}^2$ be a compact convex region under surveillance. We assume a swarm of n MAAs, each positioned at the spatial coordinates $X_i = [x_i\ y_i\ z_i]^T,\ i \in I_n$, where $I_n = \{1,\ldots,n\}$. We also define the vector $q_i = [x_i\ y_i]^T,\ q_i \in \Omega$ to note the projection of the center of each MAA on the ground. The minimum and maximum altitudes each MAA can fly to are $z_i^{\min}$ and $z_i^{\max}$ respectively, thus $z_i \in [z_i^{\min},\ z_i^{\max}],\ i \in I_n$. It is also assumed that $z_i^{\min} > 0,\ \forall i \in I_n$, since setting the minimum altitude to zero could potentially cause some MAAs to crash.

The simplified MAA's kinodynamic model is

$$\begin{aligned} \dot{q}_i &= u_{i,q},\ q_i \in \Omega,\ u_{i,q} \in \mathbb{R}^2, \\ \dot{z}_i &= u_{i,z},\ z_i \in [z_i^{\min}\ ,\ z_i^{\max}],\ u_{i,z} \in \mathbb{R}. \end{aligned} \tag{1}$$

where $[u_{i,q}, u_{i,z}]$ is the corresponding 'thrust' control input for each MAA (node). The minimum altitude $z_i^{\min}$ is used to ensure the MAAs will fly above ground obstacles, whereas the maximum altitude $z_i^{\max}$ guarantees that they will not fly out of range of their base station. In the sequel, all MAAs are assumed to have common minimum $z^{\min}$ and maximum $z^{\max}$ altitudes.

As far as the sensing performance of the MAAs (nodes) is concerned, all members are assumed to be equipped with identical downwards pointing sensors with conic sensing patterns. Thus the region of Ω sensed by each node is a disk defined as

$$C_i^s(X_i, a) = \{q \in \Omega :\| q - q_i \| \leq z_i \tan a\},\ i = 1,\ldots,n, \tag{2}$$

where a is half the angle of the sensing cone. As shown in Figure 1, the higher the altitude of an MAA, the larger the area of Ω surveyed by its sensor.

The coverage quality of each node is a function $f(z_i)\colon [z^{\min},\ z^{\max}] \to [0,1]$ which is dependent on the node's altitude constraints $z^{\min}$ and $z^{\max}$. The coverage quality of node i is assumed to be uniform throughout its sensed region C_i^s. The higher the value of $f(z_i)$, the better the coverage quality. It is assumed that as the altitude of a node increases, the visual quality of its sensed area decreases. The exact definition and properties of $f(z_i)$ are presented in Section 3.

For each point $q \in \Omega$, an importance weight is assigned via the space density function $\phi : \Omega \to \mathbb{R}^+$, encapsulating any a priori information regarding the region of interest. Thus the coverage-quality objective is

$$\mathscr{H} \triangleq \int_{\Omega} \max_{i \in I_n} f(z_i)\ \phi(q)\ dq. \tag{3}$$

In the sequel, we assume $\phi(q) = 1,\ \forall q \in \Omega$ but the expressions can be easily altered to take into account any a priori weight function.

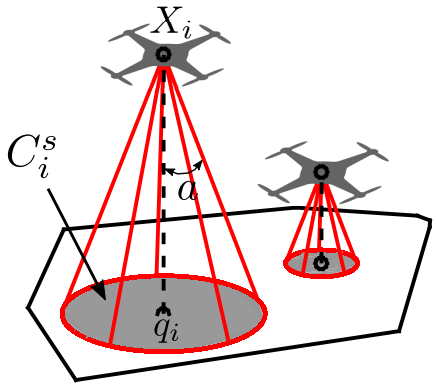

Figure 1: MAA-visual area coverage concept

3. Coverage quality function

A uniform coverage quality throughout the sensed region C_i^s can be used to model downward facing cameras [24, 25] that provide uniform quality in the whole image. The uniform coverage quality function $f(z_i) : [z^{\min},\ z^{\max}] \to [0,1]$ was chosen to be

$$f(z_i) = \begin{cases} \dfrac{\left(\left(z_i - z^{\min}\right)^2 - \left(z^{\max} - z^{\min}\right)^2\right)^2}{\left(z^{\max} - z^{\min}\right)^4}, & q \in C_i^s \\ 0, & q \notin C_i^s \end{cases}$$

A plot of this function can be seen in Figure 2 [Left]. This function was chosen so that $f(z^{\min}) = 1$ and $f(z^{\max}) = 0$. In addition, $f(z_i)$ is first order differentiable with respect to z_i, or $\frac{\partial f(z_i)}{\partial z_i}$ exists within C_i^s, which is a property that will be required when deriving the control law in Section 5.

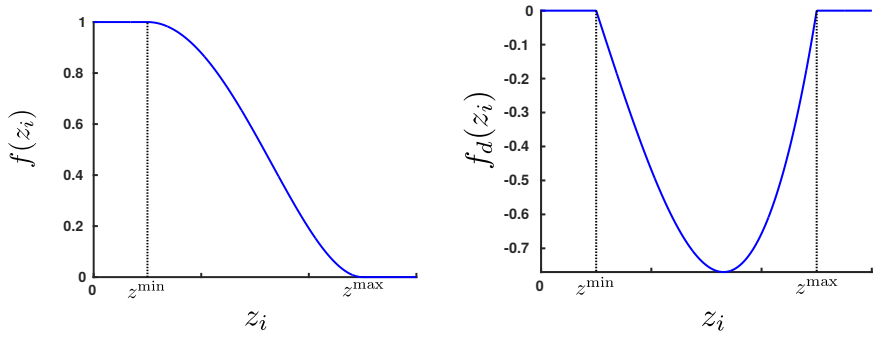

Figure 2: Uniform coverage quality function [Left] and its derivative [Right].

The derivative $\frac{\partial f(z_i)}{\partial z_i}\colon [z^{\min},\ z^{\max}] \to [f_d^{\min}, 0]$ is evaluated as

$$f_d(z_i) \triangleq \frac{\partial f(z_i)}{\partial z_i} = \begin{cases} \dfrac{4\left(z_i - z^{\min}\right)\left[\left(z_i - z^{\min}\right)^2 - \left(z^{\max} - z^{\min}\right)^2\right]}{\left(z^{\max} - z^{\min}\right)^4}, & q \in C_i^s \\ 0, & q \notin C_i^s \end{cases}$$

where $f_d^{\min} = f_d\left(z^{\min} + \frac{\sqrt{3}}{3}\left(z^{\max} - z^{min}\right)\right) = -\frac{8\sqrt{3}}{9\left(z^{\max} - z^{min}\right)}$. A plot of this function can be seen in Figure 2 [Right].

$f(z_i)$ and $f_d(z_i)$ are 4th and 3rd degree polynomials respectively and as a result continuous functions of z_i. It should be noted that any strictly decreasing and differentiable with a continuous derivative function $f(z_i)\colon [z^{\min},\ z^{\max}] \to [0,1]$ can be potentially used.

4. Sensed space partitioning

The assignment of responsibility regions to the nodes is achieved in a manner similar to [12], where only the subset of Ω sensed by the nodes is partitioned. Each node is assigned a cell

$$W_i \triangleq \left\{q \in \Omega\colon f(z_i) \geq f(z_j),\ j \neq i\right\} \tag{4}$$

with the equality holding true only at the boundary ∂W_i, so that the cells W_i comprise a complete tessellation of the sensed region.

Because the coverage quality is uniform, $\partial W_j \cap \partial W_i$ is either an arc of ∂C_i if $z_i < z_j$ or of ∂C_j if $z_i > z_j$. In the case where $z_i = z_j$, $\partial W_j \cap \partial W_i$ is chosen arbitrarily as the line segment defined by the two intersection points of ∂C_i and ∂C_j. Hence, the resulting cells consist of circular arcs and line segments.

If the sensing disk of a node i is contained within the sensing disk of another node j, i.e. $C_i^s \cap C_j^s = C_i^s$, then $W_i = C_i^s$ and $W_j = C_j^s \setminus C_i^s$. An example partitioning with all of the aforementioned cases illustrated can be seen in Figure 3 [Left], where the boundaries of the sensing disks ∂C_i^s are in dashed and the boundaries of the cells ∂W_i in solid black. Nodes 1 and 2 are at the same altitude so the arbitrary partitioning scheme is used. The sensing disk of node 3 contains the sensing disk of node 4 and nodes $5, 6$ and 7 illustrate the general case.

By utilizing this partitioning scheme, the network's coverage performance can be written as

$$\mathscr{H} = \sum_{i \in I_n} \int_{W_i} f(z_i)\ \phi(q)\ dq. \tag{5}$$

Definition 1. *We define the neighbors N_i of node i as*

$$N_i \stackrel{\triangle}{=} \left\{ j \neq i \colon C_j^s \cap C_i^s \neq \emptyset \right\}.$$

The neighbors of node i are those nodes that sense at least a part of the region that node i senses. It is clear that, due to the partitioning scheme used, only the nodes in N_i need to be considered when creating W_i.

Remark 1. The aforementioned partitioning is a complete tessellation of the sensed region $\bigcup_{i \in I_n} C_i^s$. However it is not a complete tessellation of Ω. The neutral region not assigned by the partitioning scheme is denoted as $\mathscr{O} = \Omega \setminus \bigcup_{i \in I_n} W_i$.

Remark 2. The resulting cells W_i are compact but they are not always convex. It is also possible that a cell W_i consists of multiple disjoint regions, such as the cell of node 1 shown in red in Figure 3 [Right]. In addition it is possible that the cell of a node is empty, such as the cell of node 8 in Figure 3 [Right]. Its sensing circle ∂C_8^s is shown in a solid red line.

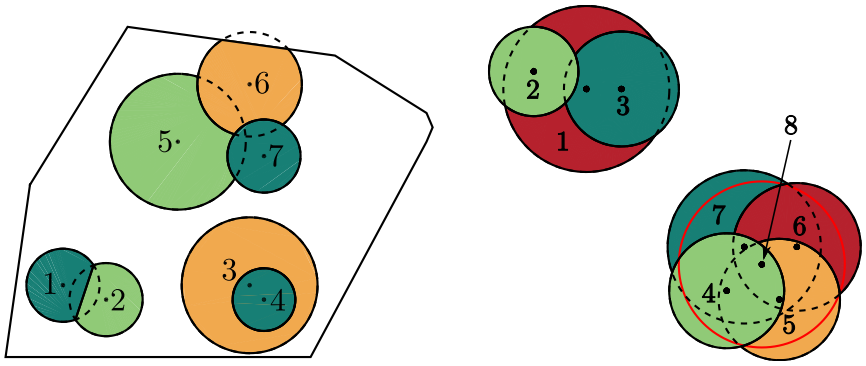

Figure 3: Space partitioning examples.

5. Spatially Distributed Coordination Algorithm

Based on the nodes kinodynamics (1), their sensing performance (2) and the coverage criterion (5), a gradient based control law is designed. The control law utilizes the partitioning (4) and result in monotonous increase of the covered area.

Theorem 1. *In an MAA visual network consisting of nodes with sensing performance as in (2), governed by the kinodynamics in (1) and the space partitioning described in Section 4, the control law*

$$u_{i,q} = \alpha_{i,q}\left[\int_{\partial W_i \cap \partial \mathscr{O}} n_i\, f(z_i)\, dq + \sum_{j\neq i}\int_{\partial W_i \cap \partial W_j} \upsilon_i^i\, n_i\, (f(z_i) - f(z_j))\, dq\right] \tag{6}$$

$$u_{i,z} = \alpha_{i,z}\left[\int_{\partial W_i \cap \partial \mathscr{O}} \tan(a)\, f(z_i)\, dq + f_d(z_i)\int_{W_i} dq + \sum_{j\neq i}\int_{\partial W_i \cap \partial W_j} \nu_i^i \cdot n_i\, (f(z_i) - f(z_j))\, dq\right] \tag{7}$$

where $\alpha_{i,q}, \alpha_{i,z}$ are positive constants, υ_i^i and ν_i^i are the Jacobian matrices of the points $q \in \partial W_i$ with respect to q_i and z_i respectively and n_i the outward pointing normal vector of W_i, maximizes the performance criterion (5) monotonically along the nodes' trajectories, leading in a locally optimal configuration.

PROOF. Initially we evaluate the time derivative of the optimization criterion $\mathscr{H}$

$$\frac{d\mathscr{H}}{dt} = \sum_{i\in I_n}\left[\frac{\partial \mathscr{H}}{\partial q_i}\dot{q}_i + \frac{\partial \mathscr{H}}{\partial z_i}\dot{z}_i\right] = \sum_{i\in I_n}\left[\frac{\partial \mathscr{H}}{\partial q_i}u_{i,q} + \frac{\partial \mathscr{H}}{\partial z_i}u_{i,z}\right].$$

.

The usage of a gradient based control law in the form

$$u_{i,q} = \alpha_{i,q}\frac{\partial \mathscr{H}}{\partial q_i},\ \ u_{i,z} = \alpha_{i,z}\frac{\partial \mathscr{H}}{\partial z_i}$$

will result in a monotonous increase of $\mathscr{H}$.

By using the Leibniz integral rule [26] we obtain

$$\begin{aligned}\frac{\partial \mathscr{H}}{\partial q_i} &= \sum_{i\in I_n}\left[\int_{\partial W_i} \upsilon_i^i\, n_i\, f(z_i)\, dq + \int_{W_i}\frac{\partial f(z_i)}{\partial q_i}\, dq\right] \\ &= \int_{\partial W_i} \upsilon_i^i\, n_i\, f(z_i)\, dq + \int_{W_i}\frac{\partial f(z_i)}{\partial q_i}\, dq + \sum_{j\neq i}\left[\int_{\partial W_j} \upsilon_j^i\, n_j\, f(z_j)\, dq + \int_{W_j}\frac{\partial f(z_j)}{\partial q_i}\, dq\right]\end{aligned}$$

where υ_j^i stands for the Jacobian matrix with respect to q_i of the points $q \in \partial W_j$,

$$\upsilon_j^i(q) \triangleq \frac{\partial q}{\partial q_i},\ \ q \in \partial W_j,\ i,j \in I_n. \tag{8}$$

Since $\frac{\partial f(z_i)}{\partial q_i} = \frac{\partial f(z_j)}{\partial q_i} = 0$ we obtain

$$\frac{\partial \mathscr{H}}{\partial q_i} = \int_{\partial W_i} \upsilon_i^i\, n_i\, f(z_i)\, dq + \sum_{j\neq i}\int_{\partial W_j} \upsilon_j^i\, n_j\, f(z_j)\, dq$$

whose two terms indicate how a movement of node i affects the boundary of its cell and the boundaries of the cells of other nodes. It is clear that only the cells W_j which have a common boundary with W_i will be affected and only at that common boundary.

The boundary ∂W_i can be decomposed in disjoint sets as

$$\partial W_i = \{\partial W_i \cap \partial\Omega\} \cup \{\partial W_i \cap \partial\mathscr{O}\} \cup \{\bigcup_{j\neq i}(\partial W_i \cap \partial W_j)\}. \tag{9}$$

These sets represent the parts of ∂W_i that lie on the boundary of Ω, the boundary of the node's sensing region and the parts that are common between the boundary of the cell of node i and those of other nodes. This decomposition can be seen in Figure 4 with the sets $\partial W_i \cap \partial\Omega$, $\partial W_i \cap \partial\mathscr{O}$ and $\partial W_i \cap \bigcup_{j\neq i}\partial W_j$ appearing in solid red, green and blue respectively.

At $q \in \partial\Omega$ it holds that $\upsilon_i^i = \mathbf{0}_{2\times 2}$ since we assume the region of interest is static. Additionally, since only the common boundary $\partial W_j \cap \partial W_i$ of node i with any other node j is affected by the movement of node i, $\frac{\partial \mathscr{H}}{\partial q_i}$ can be simplified as

$$\frac{\partial \mathscr{H}}{\partial q_i} = \int_{\partial W_i\cap\partial\mathscr{O}} \upsilon_i^i\, n_i\, f(z_i)\, dq + \sum_{j\neq i}\int_{\partial W_i\cap\partial W_j} \upsilon_i^i\, n_i\, f(z_i)\, dq + \sum_{j\neq i}\int_{\partial W_j\cap\partial W_i} \upsilon_j^i\, n_j\, f(z_j)\, dq.$$

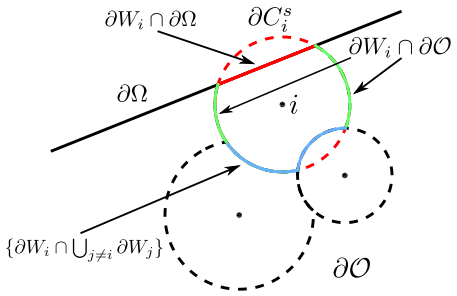

Figure 4: ∂W_i-decomposition into disjoint sets

The evaluation of υ_i^i can be found in Appendix A. Because the boundary $\partial W_i \cap \partial W_j$ is common among nodes i and j, it holds true that $\upsilon_j^i = \upsilon_i^i$ when evaluated over it and that $n_j = -n_i$. Finally, the sums and the integrals within them can be combined, producing the final form of the planar control law

$$\frac{\partial \mathscr{H}}{\partial q_i} = \int\limits_{\partial W_i \cap \partial \mathscr{O}} n_i\, f(z_i)\, dq + \sum_{j\neq i} \int\limits_{\partial W_j \cap \partial W_i} \upsilon_i^i\, n_i\, \left(f(z_i) - f(z_j)\right)\, dq.$$

Similarly, by using the same ∂W_i decomposition and defining $\nu_j^i(q) \triangleq \frac{\partial q}{\partial z_i}$, $q \in \partial W_j,\ i,j \in I_n$, the altitude control law is

$$\frac{\partial \mathscr{H}}{\partial z_i} = \int\limits_{\partial W_i \cap \partial \mathscr{O}} \nu_i^i \cdot n_i\, f(z_i)\, dq + \int\limits_{W_i} \frac{\partial f(z_i)}{\partial z_i}\, dq + \sum_{j\neq i} \int\limits_{\partial W_j \cap \partial W_i} \nu_i^i \cdot n_i\, \left(f(z_i) - f(z_j)\right)\, dq$$

where the evaluation of $\nu_i^i(q) \cdot n_i$ on $\partial W_i \cap \partial \mathscr{O}$ and $\partial W_j \cap \partial W_i$ can also be found in Appendix A. Because $\frac{\partial f(z_i)}{\partial z_i}$ is constant over W_i and using the expression for $\nu_i^i(q) \cdot n_i$ from Appendix A, the control law can be further simplified into

$$\frac{\partial \mathscr{H}}{\partial z_i} = \int\limits_{\partial W_i \cap \partial \mathscr{O}} \tan(a)\, f(z_i)\, dq + f_d(z_i) \int\limits_{W_i} dq + \sum_{j\neq i} \int\limits_{\partial W_j \cap \partial W_i} \nu_i^i \cdot n_i\, \left(f(z_i) - f(z_j)\right)\, dq.$$

Remark 3. The cell W_i of node i is affected only by its neighbors N_i thus resulting in a distributed control law. The discovery of the neighbors N_i depends on their coordinates $X_j,\ j \in N_i$ and does not correspond to the classical 2D-Delaunay neighbor search. The computation of the N_i set demands node i to be able to communicate with all nodes within a sphere centered around X_i and radius r_i^c

$$r_i^c = \max\left\{2\, z_i\, \tan a,\ \left(z_i + z^{\min}\right)^2 \tan^2 a + \left(z_i - z^{\min}\right)^2,\ \left(z_i + z^{\max}\right)^2 \tan^2 a + \left(z_i - z^{\max}\right)^2\right\}.$$

Figure 5 highlights the case where nodes 2, 3 and 4 are at $z^{\min}$, z_1 and $z^{\max}$ respectively. These are the worst case scenario neighbors of node 1 , the farthest of which dictates the communication range r_1^c.

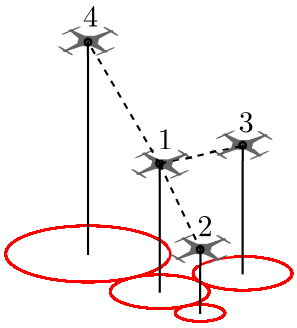

Figure 5: N_i neighbor set

Remark 4. When $z_i = z^{\max}$, both the planar and altitude control laws are zero because $f(z_i) = 0$. This results in the MAA being unable to move any further in the future and additionally its contribution to the coverage-quality objective being zero. However this degenerate case is of little concern, as shown in Sections 6.3 and 6.4.

Remark 5. The control law essentially maximizes the volume contained by the union of all the cylinders defined by $f(z_i),\ i \in I_n$, under the constraints imposed by the network and area of interest.

6. MAA Altitude Stability

In this section we examine the stability of the nodes' altitude z_i and show that it always remains in the interval $[z^{\min},\ z^{\max}]$. The system under examination is

$$\dot{z}_i = u_{i,z},\ u_{i,z} \in \mathbb{R}.$$

We will first find and characterize its equilibrium points for the case of a single node and then generalize to the case of multiple nodes.

6.1. Optimal altitude for a single MAA

It is useful to define an optimal altitude z^{opt} as the altitude a node would reach if: 1) it had no neighbors ($N_i = \varnothing$), and 2) its whole cell was inside the region of interest ($\Omega \cap W_i = W_i$). When the aforementioned requirements are met it holds true that $W_i = C_i^s$. This optimal altitude is the stable equilibrium point of the system

$$\dot{z}_i = u_{i,z}^{opt},\ u_{i,z}^{opt} \in \mathbb{R}$$

where

$$u_{i,z}^{opt} = \int\limits_{\partial C_i^s} \tan(a)\ f(z_i)\ dq\ + f_d(z_i) \int\limits_{C_i^s} dq = 2\pi\ \tan^2(a)\ z_i f(z_i)\ + \pi\ \tan^2(a)\ z_i^2\ f_d(z_i)$$

Its value and stability are examined in the following section. This altitude is constant and depends solely on the network's parameters $z^{\min}$ and $z^{\max}$. Had we allowed the nodes to have different minimum and maximum altitudes, each node would have a different constant optimal altitude z_i^{opt}.

Additionally, let us denote the sensing region of a node i at z^{opt} as $C_{i,opt}^s\left([x_i\ y_i\ z_i^{opt}]^T, a\right)$ and $\mathscr{H}_{opt}$ the value of the criterion when all nodes are located at z^{opt}.

If $\Omega = \mathbb{R}^2$ and because the planar control law $u_{i,q}$ results in the repulsion of the nodes, the network will reach a state in which no node will have neighbors and all nodes will be at z^{opt}. In that state, the coverage-quality criterion (5) will have attained its maximum possible value $\mathscr{H}_{opt}$ for that particular network configuration and coverage quality function f. This network configuration will be globally optimal.

When Ω is a convex compact subset of $\mathbb{R}^2$, it is possible for the network to reach a state where all the nodes are at z^{opt} only if n $C_{i,opt}^s$ disks can be packed inside Ω. This state will be globally optimal. If that is not the case, the nodes will converge at some altitude other than z^{opt} and in general different among nodes. It should be noted that although the nodes do not reach z^{opt}, the network configuration is locally optimal.

6.2. Optimal altitude stability

We will now evaluate z^{opt} and its stability properties. The system under examination is

$$\dot{z}_i \quad = \quad u_{i,z}^{opt}.$$

In Appendix B it is shown that out of the five equilibrium points of this system, only two reside in the interval $[z^{\min},\, z^{\max}]$. Those are

$$\begin{aligned} z_2^{eq} &= z^{\max} \\ z_5^{eq} &= \frac{2}{3}\, z^{\min} + \frac{1}{3}\sqrt{Q} \end{aligned}$$

where

$$Q = 3\, z^{\max 2} - 6\, z^{\max}\, z^{\min} + 4\, z^{\min 2} = 3\left(z^{\max} - z^{\min}\right)^2 + z^{\min 2} = P + z^{\min 2} > 0. \quad (10)$$

Because the system is scalar, in order to evaluate the stability of those two equilibrium points, it is sufficient to consider the sign of $u_{i,z}^{opt}$ in the interval $[z^{\min},\, z^{\max}]$. Since $u_{i,z}^{opt}$ is continuous in $[z^{\min},\, z^{\max}]$, its sign will be constant between consecutive roots of $u_{i,z}^{opt} = 0$. It is shown in Appendix C that

$$\begin{aligned} u_{i,z}^{opt} &> 0, \quad \forall z_i \in \left[z^{\min}, z_5^{eq}\right) \\ u_{i,z}^{opt} &< 0, \quad \forall z_i \in \left(z_5^{eq}, z^{\max}\right). \end{aligned}$$

This can also be seen in Figure 6 where $u_{i,z}^{opt}(z_i)$ is shown in blue, the integral over W_i in green and the integral over ∂W_i in red.

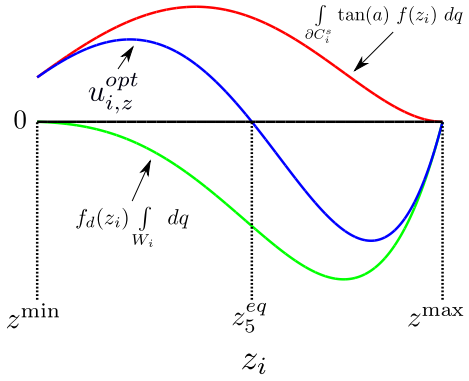

Figure 6: Plot of $u_{i,z}^{opt}$ and its terms over W_i and ∂W_i with respect to z_i.

It can now be shown that the equilibrium point $z^{\max}$ is unstable because a small negative disturbance dz will result in $u_{i,z}^{opt} < 0$, thus leading the node to a lower altitude and away from $z^{\max}$.

Similarly, the equilibrium point z_5^{eq} is asymptotically stable. This is because a small negative disturbance dz will result in $u_{i,z}^{opt} > 0$, thus leading the node to a higher altitude and closer to z_5^{eq}. Conversely, a small positive disturbance dz will result in $u_{i,z}^{opt} < 0$, thus leading the node to a lower altitude and again closer to z_5^{eq}.

To conclude, when a node has no neighbors and its whole cell is inside Ω, the only stable equilibrium point is $z^{opt} = z_5^{eq}$ which has a domain of attraction $[z^{\min},\ z^{\max})$.

6.3. Stable altitude for a team of MAAs

In the general case, each node will move towards an altitude which is an equilibrium point of the system

$$\dot{z}_i = u_{i,z},\ u_{i,z} \in \mathbb{R} \tag{11}$$

where

$$u_{i,z} = \int\limits_{\partial W_i \cap \partial \mathscr{O}} \tan(a)\ f(z_i)\ dq + f_d(z_i) \int\limits_{W_i} dq + \sum_{j \neq i} \int\limits_{\partial W_i \cap \partial W_j} \tan(a)\ (f(z_i) - f(z_j))\ dq \tag{12}$$

We call this the stable altitude z_i^{stb}. The stable altitude is not common among nodes as it depends on one's neighbors N_i and is not constant over time since the neighbors change over time.

We will attempt to generalize the proof of Section 6.2 in the case of a node with neighbors, which is the general case. The system under examination is derived from equations (11) and (12). The integrals over ∂W_i are non–negative whereas the integral over W_i is non–positive. The integrals over ∂W_i of a node with neighbors will always be smaller than the same integral of a node without neighbors. This is because the neighbors will either remove some arcs of W_i from the integral or reduce their influence due to the term $f(z_i) - f(z_j)$. Similarly, the absolute value of the integral over W_i of a node with neighbors will not be greater than the same integral of a node without neighbors. This is due to the area of W_i possibly being reduced because part of C_i^s has been assigned to neighbors with higher coverage quality. Thus we conclude that z_i^{stb} will attain its minimum value when the integrals over ∂W_i are zero and its maximum value when the integral over W_i is zero.

When the integrals over ∂W_i are both zero, the control law $u_{i,z}$ has a negative value. This will lead to a reduction of the node's altitude and in time the node will reach

$z_i^{stb} = z^{\min}$, provided the integrals over ∂W_i remain zero. Once the node reaches $z^{\min}$ its altitude control law will be 0 until the integral over ∂W_i stops being zero. The planar control law $u_{i,q}$ however is unaffected, so the node's performance in the future is not affected. This situation may arise in a node with several neighboring nodes at lower altitude that result in $\partial C_i^s \cap \partial W_i = \emptyset$.

When the integral over W_i is zero, the control law $u_{i,z}$ has a positive value. This will lead to an increase of the node's altitude and in time the node will reach $z_i^{stb} = z^{\max}$ and as shown in Remark 4 the node will be immobilized from this time onwards. However this situation will not arise in practice as explained in Section 6.4.

When the integral over W_i and at least one of the integrals over ∂W_i are non-zero, then $z_i^{stb} \in \left(z^{\min}, z^{\max}\right)$.

The stability of z_i^{stb} is shown similarly to the stability of z^{opt}, by using the sign of $u_{i,z}$.

6.4. Degenerate cases

It is possible due to the nodes' initial positions that the sensing disk of some node i is completely contained within the sensing disk of another node j, i.e. $C_i^s \cap C_j^s = C_i^s$. In such a case, it is not guaranteed that the control law will result in separation of the nodes' sensing regions and thus it is possible that the nodes do not reach z^{opt}. Instead, node j may converge to a higher altitude and node i to a lower altitude than z^{opt}, while their projections on the ground q_i and q_j remain stationary. Because the region covered by node i is also covered by node j, the network's performance is impacted negatively. Since this degenerate case may only arise at the network's initial state, care must be taken to avoid it during the agents' deployment. Such a degenerate case is shown in Figure 3 [Left] where the sensing disk of node 4 is completely contained within that of node 3.

Another case of interest is when some node i is not assigned a region of responsibility, i.e. $W_i = \emptyset$. This is due to the existence of other nodes at lower altitude that cover all of C_i^s with better quality than node i. This is the case with node 8 in Figure 3 [Right]. This situation is resolved since the nodes at lower altitude will move away from node i and once node i has been assigned a region of responsibility it will also

move. It should be noted that the coverage objective $\mathscr{H}$ remains continuous even when node i changes from being assigned no region of responsibility to being assigned some region of responsibility.

In order for a node to reach $z^{\max}$, as explained in Section 6.3, the integral over W_i of its altitude control law $u_{i,z}$ must be zero, that is its cell must consist of just a closed curve without its interior. In order to have $W_i = \partial W_i$, a second node j must be directly below node i at an infinitesimal distance. However just as node i starts moving upwards the integral over W_i will stop being zero thus changing the stable altitude to some value $z_i^{stb} < z^{\max}$. In other words, in order for a node to reach $z^{\max}$, the configuration described must happen at an altitude infinitesimally smaller than $z^{\max}$. So in practice, if all nodes are deployed initially at an altitude smaller than $z^{\max}$, no node will reach $z^{\max}$ in the future.

7. Simulation Studies

Simulation results of the proposed control law using the uniform coverage quality function f are presented in this section. The region of interest Ω is the same as the one used in [3] for consistency. All nodes are identical with a half sensing cone angle $a = 20^\circ$ and $z_i \in [0.5,\ 2.5],\ \forall i \in I_n$. The boundaries of the nodes' cells are shown in solid black and the boundaries of their sensing disks in dashed red lines.

Remark 6. It is possible to observe jittering on the cells of some nodes i and j. This can happen when $z_i = z_j$ and the arbitrary boundary $\partial W_i \cap \partial W_j$ is used. Once the altitude of one of the nodes changes slightly, the boundary between the cells will change instantaneously from a line segment to a circular arc. The coverage-quality objective $\mathscr{H}$ however will present no discontinuity when this happens.

7.1. Case Study I

In this simulation three nodes start grouped as seen in Figure (7) [Left]. Since the region of interest is large enough for three optimal disks $C^s_{i,opt}$ to fit inside, all the nodes converge at the optimal altitude z^{opt}. As it can be seen in Figure 10, the area covered by the network is equal to $\mathscr{A}\left(\bigcup_{i\in I_n} C^s_{i,opt}\right)$ and the coverage-quality criterion has reached

$\mathscr{H}_{opt} = \mathscr{A}\left(\bigcup_{i\in I_n} C^s_{i,opt}\right)$. However since all nodes converged at z^{opt}, the addition of more nodes will result in significantly better performance coverage and quality wise, as is clear from Figure 7 [Right] and Figure 10 [Left]. Figure 8 shows a graphical representation of the coverage quality at the initial and final stages of the simulation. It is essentially a plot of all $f(z_i)$ inside the region of interest. The volume of the cylinders in Figure 8 [Right] is the maximum possible. The trajectories of the MAAs in $\mathbb{R}^3$ can be seen in Figure 9 in red and their projections on the region of interest in black. The initial positions of the MAAs are marked by squares and their final positions by circles.

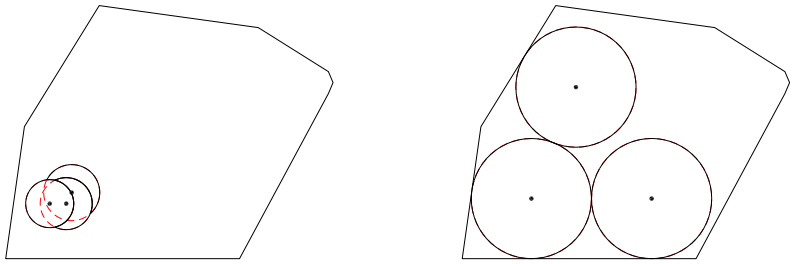

Figure 7: Initial [Left] and final [Right] network configuration and space partitioning.

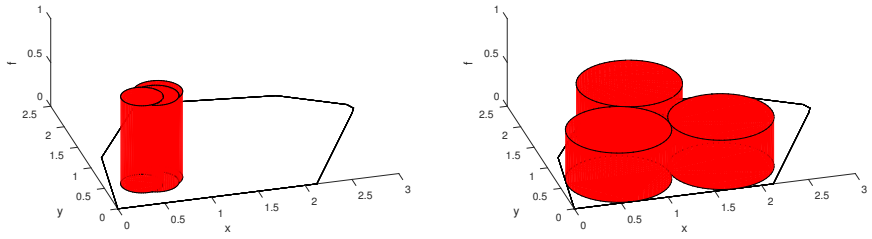

Figure 8: Initial [Left] and final [Right] coverage quality.

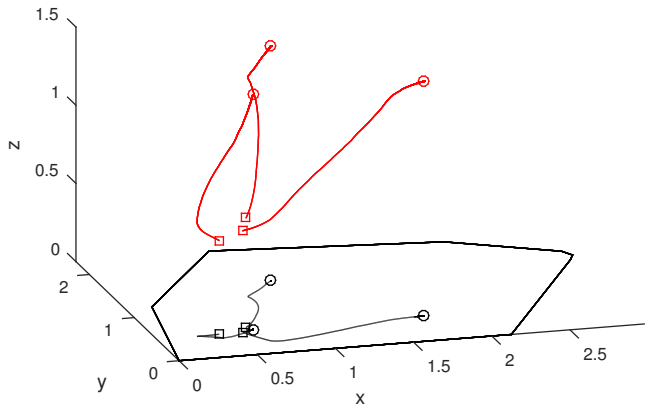

Figure 9: Node trajectories (blue) and their projections on the sensed region (black).

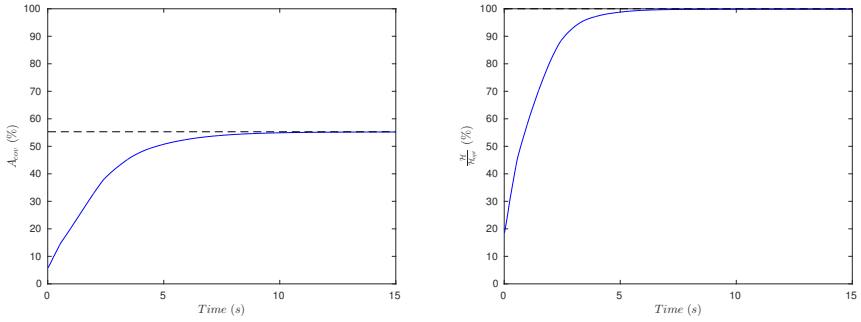

Figure 10: $\frac{\mathscr{A}\left(\bigcup_{i\in I_n} C_i^s\right)}{\mathscr{A}(\Omega)}$ [Left] and $\frac{\mathscr{H}}{\mathscr{H}_{opt}}$ [Right].

7.2. Case Study II

A network of nine nodes, identical to those in Case Study I, is examined in this simulation with an initial configuration as seen in Figure 11 [Left]. The region Ω is not large enough to contain these nine $C^s_{i,opt}$ disks and so the nodes converge at different altitudes below z^{opt}. This is why the covered area never reaches $\mathscr{A}\left(\bigcup_{i\in I_n} C^s_{i,opt}\right)$, which is larger than $\mathscr{A}(\Omega)$ and why $\mathscr{H}$ never reaches $\mathscr{H}_{opt}$, as seen in Figure 14. It can be clearly seen though from Figure 11 [Right] and Figure 14 [Left] that the network covers a significant portion of Ω with better quality than Case Study I. The volume of the cylinders in Figure 12 [Right] has reached a local optimum. The trajectories of the MAAs in $\mathbb{R}^3$ can be seen in Figure 13 in red and their projections on the region of interest in black. The initial positions of the MAAs are marked by squares and their final positions by circles. It can be seen from the trajectories that the altitude of some nodes was not constantly increasing. This is expected behavior since nodes at lower altitude will increase the stable altitude of nodes at higher altitude they share sensed regions with. Once they no longer share sensed regions, or share a smaller portion, the stable altitude of the upper node will decrease, leading to a decrease in their altitude.

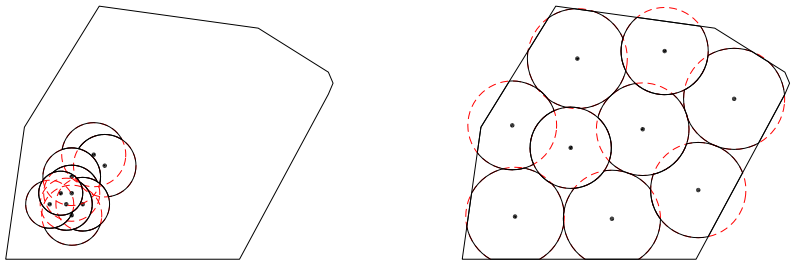

Figure 11: Initial [Left] and final [Right] network configuration and space partitioning.

8. Conclusions

Area coverage by a network of MAAs has been studied in this article by use of a combined coverage-quality metric. A partitioning scheme based on coverage quality

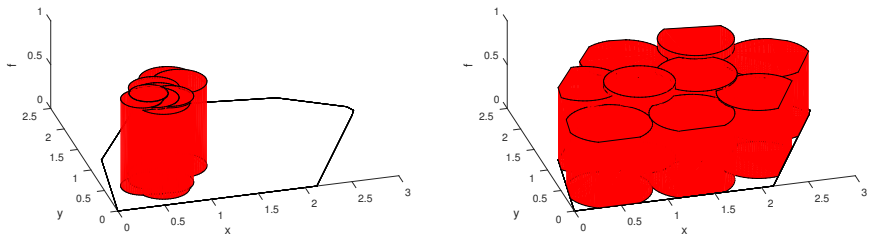

Figure 12: Initial [Left] and final [Right] coverage quality.

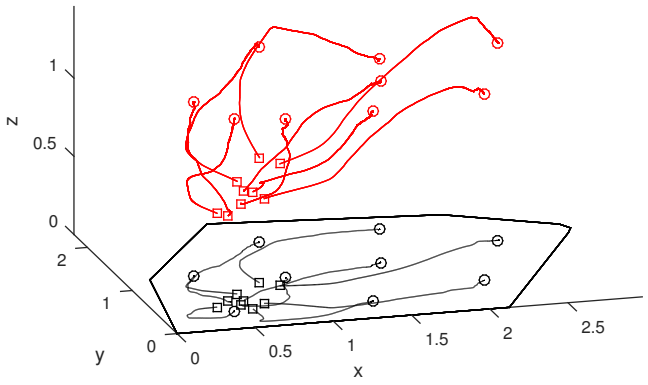

Figure 13: Node trajectories (blue) and their projections on the sensed region (black).

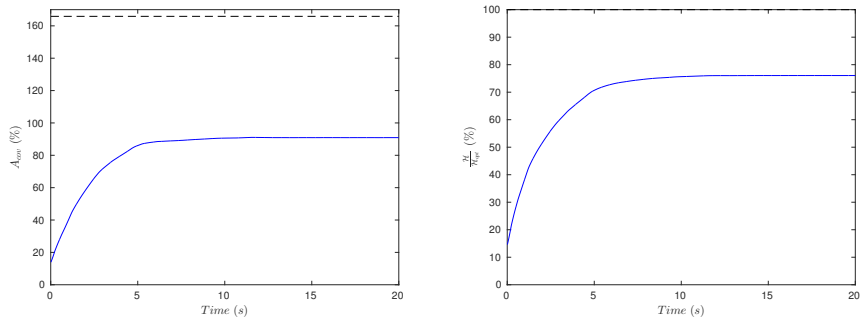

Figure 14: $\frac{\mathscr{A}\left(\bigcup_{i\in I_n} C_i^s\right)}{\mathscr{A}(\Omega)}$ [Left] and $\frac{\mathscr{H}}{\mathscr{H}_{opt}}$ [Right].

is employed to assign each MAA an area of responsibility. The proposed control law leads the network to a locally optimal configuration which provides a compromise between covered area and coverage quality. It also guarantees that the altitude of all MAAs will remain within a predefined range, thus avoiding potential obstacles while also keeping the MAAs below their maximum operational altitude and in range of their base station. Simulation studies are presented to indicate the efficiency of the proposed control algorithm.

APPENDIX A - Evaluation of Jacobian matrices

The parametric equation of the boundary of the sensing disk $C_i^s(X_i,a)$ defined in (2) is

$$\gamma_i(k):\ \begin{bmatrix} x \\ y \end{bmatrix} = \begin{bmatrix} x_i + z_i \tan(a)\ \cos(k) \\ y_i + z_i \tan(a)\ \sin(k) \end{bmatrix},\ k \in [0, 2\pi)$$

We will first evaluate n_i, $\upsilon_i^i(q)$ and $\nu_i^i(q)$ on $\partial W_i \cap \partial \mathscr{O}$ which is always an arc of the circle $\gamma_i(k)$ because of the partitioning scheme (4). The normal vector n_i is given by

$$n_i = \begin{bmatrix} \cos(k) \\ \sin(k) \end{bmatrix},\ k \in [0, 2\pi).$$

It can be shown that

$$\upsilon_i^i(q) = \begin{bmatrix} \frac{\partial x}{\partial x_i} & \frac{\partial x}{\partial y_i} \\ \frac{\partial y}{\partial x_i} & \frac{\partial y}{\partial y_i} \end{bmatrix} = \begin{bmatrix} 1 & 0 \\ 0 & 1 \end{bmatrix} = \mathbb{I}_2$$

and similarly that

$$v_i^i(q) = \begin{bmatrix} \frac{\partial x}{\partial z_i} \\ \frac{\partial y}{\partial z_i} \end{bmatrix} = \begin{bmatrix} \tan(a)\cos(k) \\ \tan(a)\sin(k) \end{bmatrix}, \; k \in [0, 2\pi)$$

resulting in

$$v_i^i(q) \cdot n_i = \tan(a).$$

We will now evaluate n_i, $v_i^i(q)$ and $v_i^i(q)$ on $\partial W_j \cap \partial W_i$.

If $f(z_i) = f(z_j)$, the evaluation of n_i, $v_i^i(q)$ and $v_i^i(q)$ is irrelevant since the corresponding integral will be 0 due to the $f(z_i) - f(z_j)$ term.

If $f(z_i) > f(z_j)$, then according to the partitioning scheme (4), $\partial W_j \cap \partial W_i$ will be an arc of $\gamma_i(k)$. Thus the evaluation of n_i, $v_i^i(q)$ and $v_i^i(q)$ is the same as it was over $\partial W_i \cap \partial \mathscr{O}$.

If $f(z_i) < f(z_j)$, then according to the partitioning scheme (4), $\partial W_j \cap \partial W_i$ will be an arc of $\gamma_j(k)$. Thus both $v_i^i(q)$ and $v_i^i(q)$ will be 0, since $C_j^s(X_j, a)$ is not dependent on X_i.

To sum up, the evaluation of $v_i^i(q)$ and $v_i^i(q)$ over $\partial W_j \cap \partial W_i$ are the following

$$v_i^i = \begin{cases} \mathbb{I}_2, \; z_i < z_j \\ \mathbf{0}_2, \; z_i \geq z_j \end{cases}$$

$$v_i^i \cdot n_i = \begin{cases} \tan(a), \; z_i < z_j \\ 0, \; z_i \geq z_j \end{cases}$$

where

$$\mathbf{0}_2 = \begin{bmatrix} 0 & 0 \\ 0 & 0 \end{bmatrix}.$$

It is thus concluded that for the integrals over $\partial W_j \cap \partial W_i$ for the control law of node i, only arcs where $f(z_i) > f(z_j)$ need to be considered.

APPENDIX B - Equilibrium points

The dynamical system can be written as

$$\dot{z}_i = u_{i,z}^{opt} = \pi \, \tan^2(a) \, z_i \, [2 \, f(z_i) + z_i \, f_d(z_i)].$$

Since $f(z_i)$ and $f_d(z_i)$ are 4th and 3rd degree polynomials respectively, the system has five equilibrium points, one of them being

$$z_1^{eq} = 0. \tag{13}$$

The other four are the solutions of the 4th degree polynomial $2\ f(z_i)\ +\ z_i\ f_d(z_i) = 0$ whose analytic expressions are

$$\begin{aligned} z_2^{eq} &= z^{\max} \\ z_3^{eq} &= 2\ z^{\min} - z^{\max} \\ z_4^{eq} &= \frac{2}{3}\ z^{\min} - \frac{1}{3}\sqrt{Q} \\ z_5^{eq} &= \frac{2}{3}\ z^{\min} + \frac{1}{3}\sqrt{Q} \end{aligned}$$

where Q is defined in (10), thus all equilibrium points are real.

We will examine which of these equilibrium points reside in the interval $D = [z^{\min},\ z^{\max}]$.

Equilibrium point $z_1^{eq} = 0 \notin D$ since $z^{\min} > 0$.

Equilibrium point $z_2^{eq} = z^{\max} \in D$.

Equilibrium point $z_3^{eq} = 2\ z^{\min} - z^{\max} < z^{\min}$ thus $z_3^{eq} \notin D$.

Equilibrium point $z_4^{eq} = \frac{2}{3}\ z^{\min} - \frac{1}{3}\sqrt{Q} < z^{\min}$ thus $z_4^{eq} \notin D$.

Equilibrium point $z_5^{eq} = \frac{2}{3}\ z^{\min} + \frac{1}{3}\sqrt{Q} \in D$ since $z_5^{eq} > z^{\min}$ and $z_5^{eq} < z^{\max}$.

Thus the only equilibrium points in the interval $[z^{\min},\ z^{\max}]$ are

$$\begin{aligned} z_2^{eq} &= z^{\max} \\ z_5^{eq} &= \frac{2}{3}\ z^{\min} + \frac{1}{3}\sqrt{Q}. \end{aligned}$$

APPENDIX C - Sign of $u_{i,z}^{opt}$

Since $u_{i,z}^{opt}(z_i)$ is a fifth degree polynomial function, thus both $u_{i,z}^{opt}$ and its derivative $\frac{\partial u_{i,z}^{opt}}{\partial z_i}$ are continuous functions. As a result the sign of $u_{i,z}^{opt}$ will be constant between consecutive roots of $u_{i,z}^{opt} = 0$. Since we are interested in the sign of $u_{i,z}^{opt}$ in the interval $[z^{\min},\ z^{\max}]$ and the only roots in that interval are $z^{\max}$ and $z_5^{eq} \in (z^{\min},\ z^{\max})$, as shown

in Appendix B, we just need to evaluate the sign of $u_{i,z}^{opt}$ in the intervals $\left[z^{\min}, z_5^{eq}\right)$ and $\left(z_5^{eq}, z^{\max}\right)$.

We will show that $u_{i,z}^{opt} > 0, \quad \forall z_i \in \left[z^{\min}, z_5^{eq}\right)$ by substituting $z_i^p = \frac{z^{\min}+z_5^{eq}}{2}$ into $u_{i,z}^{opt}$. After tedious algebraic manipulations it can be shown that the inequality $u_{i,z}^{opt}(z_i^p) > 0$ is equivalent to

$$\begin{aligned}\left(9z^{\max 2} - 18z^{\max}z^{\min} + 11z^{\min 2} - 2z^{\min}\sqrt{Q}\right)\left(33z^{\max 2} - 66z^{\max}z^{\min} + 31z^{\min 2} + 2z^{\min}\sqrt{Q}\right) &> 0 \Rightarrow \\ (3P-R)\cdot(11P+R) &> 0\end{aligned}$$

where $R \stackrel{\triangle}{=} 2z^{\min}\sqrt{Q} - 2z^{\min 2}$. Since $R > 0$ and $P > 0$ from (10), we have that $11P+R > 0$ and after tedious algebraic manipulations it can be shown that $3P-R > 0$ since

$$\begin{aligned}3P - R = 9z^{\max 2} - 18z^{\max}z^{\min} + 9z^{\min 2} - 2z^{\min}\sqrt{Q} + 2z^{\min 2} &> 0 \Rightarrow \\ \left(9z^{\max 2} - 18z^{\max}z^{\min} + 11z^{\min 2}\right)^2 &> 4z^{\min 2}Q.\end{aligned}$$

Substitution of Q from (10) yields

$$27P + 8z^{\min 2} > 0$$

Thus it is proven that $u_{i,z}^{opt}(z_i^p) > 0$ and consequently that $u_{i,z}^{opt} > 0, \quad \forall z_i \in [z^{\min}, z_5^{eq}]$.

We will show that $u_{i,z}^{opt} < 0, \quad \forall z_i \in \left(z_5^{eq}, z^{\max}\right)$ by evaluating the derivative of $u_{i,z}^{opt}$ at $z^{\max}$

$$\frac{\partial u_{i,z}^{opt}}{\partial z_i}(z^{\max}) = \frac{8\pi(\tan a)^2 z^{\max 2}}{\left(z^{\max} - z^{\min}\right)^2} > 0.$$

Hence $u_{i,z}^{opt}(z^{\max}) = 0$ and $\frac{\partial u_{i,z}^{opt}}{\partial z_i}(z^{\max}) > 0$.

Since $\frac{\partial u_{i,z}^{opt}}{\partial z_i}$ is a continuous function and $\frac{\partial u_{i,z}^{opt}}{\partial z_i}(z^{\max}) > 0$, there is a region E around $z^{\max}$ inside which $\frac{\partial u_{i,z}^{opt}}{\partial z_i} > 0$. Thus $z^{\max} - \varepsilon \in E$ and $\frac{\partial u_{i,z}^{opt}}{\partial z_i} > 0, \ \forall z_i \in [z^{\max} - \varepsilon, \ z^{\max}]$, where ε is an infinitesimally small positive constant. Since $u_{i,z}^{opt}$ is an increasing function in the interval $[z^{\max} - \varepsilon, \ z^{\max}]$, it is true that

$$u_{i,z}^{opt}(z^{\max} - \varepsilon) < 0 \tag{14}$$

Since the sign of $u_{i,z}^{opt}$ is constant in the interval $\left(z_5^{eq}, z^{\max}\right)$, we obtain that $u_{i,z}^{opt} < 0, \quad \forall z_i \in \left(z_5^{eq}, z^{\max}\right)$.

References

[1] J. Cortés, S. Martinez, F. Bullo, Spatially-distributed coverage optimization and control with limited-range interactions, ESAIM: Control, Optimisation and Calculus of Variations 11 (4) (2005) 691–719.

[2] L. Pimenta, V. Kumar, R. Mesquita, G. Pereira, Sensing and coverage for a network of heterogeneous robots, in: Proc. of the 47^{th} Conference on Decision and Control, Cancun, Mexico, 2008, pp. 3947–3952.

[3] Y. Stergiopoulos, A. Tzes, Convex Voronoi-inspired space partitioning for heterogeneous networks: A coverage-oriented approach, IET Control Theory and Applications 4 (12) (2010) 2802–2812.

[4] O. Arslan, D. E. Koditschek, Voronoi-based coverage control of heterogeneous disk-shaped robots, in: 2016 IEEE International Conference on Robotics and Automation (ICRA), IEEE, 2016, pp. 4259–4266.

[5] M. T. Nguyen, L. Rodrigues, C. S. Maniu, S. Olaru, Discretized optimal control approach for dynamic multi-agent decentralized coverage, in: Proc. IEEE Int. Symp. Intelligent Control (ISIC), Zadar, Croatia, 2016, pp. 1–6.

[6] M. T. Nguyen, C. S. Maniu, Voronoi based decentralized coverage problem: From optimal control to model predictive control, in: Proc. 24th Mediterranean Conf. Control and Automation (MED), Athens, Greece, 2016, pp. 1307–1312.

[7] F. Mohseni, A. Doustmohammadi, M. B. Menhaj, Distributed receding horizon coverage control for multiple mobile robots, IEEE Systems Journal 10 (1) (2016) 198–207. doi:10.1109/JSYST.2014.2325219.

[8] V. Ramaswamy, J. R. Marden, A sensor coverage game with improved efficiency guarantees, in: Proc. American Control Conf. (ACC), Boston, MA, USA, 2016, pp. 6399–6404.

[9] Y. Stergiopoulos, A. Tzes, Spatially distributed area coverage optimisation in mobile robotic networks with arbitrary convex anisotropic patterns, Automatica 49 (1) (2013) 232–237.

[10] Y. Kantaros, M. Thanou, A. Tzes, Distributed coverage control for concave areas by a heterogeneous robot-swarm with visibility sensing constraints, Automatica 53 (2015) 195–207.

[11] D. Panagou, D. M. Stipanovic, P. G. Voulgaris, Distributed dynamic coverage and avoidance control under anisotropic sensing, IEEE Transactions on Control of Network Systems PP (99) (2016) 1. doi:10.1109/TCNS.2016.2576403.

[12] Y. Stergiopoulos, A. Tzes, Cooperative positioning/orientation control of mobile heterogeneous anisotropic sensor networks for area coverage, in: Proc. IEEE International Conference on Robotics & Automation, Hong Kong, China, 2014, pp. 1106–1111.

[13] E. Bakolas, Distributed partitioning algorithms for multi-agent networks with quadratic proximity metrics and sensing constraints, Systems & Control Letters 91 (2016) 36–42.

[14] Y. Stergiopoulos, M. Thanou, A. Tzes, Distributed collaborative coverage-control schemes for non-convex domains, IEEE Transactions on Automatic Control 60 (9) (2015) 2422–2427.

[15] R. J. Alitappeh, K. Jeddisaravi, F. G. Guimarães, Multi-objective multi-robot deployment in a dynamic environment, Soft Computing (2016) 1–17.

[16] A. Renzaglia, L. Doitsidis, E. Martinelli, E. Kosmatopoulos, Muti-robot three-dimensional coverage of unknwon areas, The International Journal of Robotics Research 31 (6) (2012) 738–752.

[17] A. Breitenmoser, J. Metzger, R. Siegwart, D. Rus, Distributed coverage control on surfaces in 3d space, in: Proc. of the 2010 IEEE International Conference on Intelligent Robots and Systems, Taipei, Taiwan, 2010, pp. 5569–5576.

[18] M. Thanou, A. Tzes, Distributed visibility-based coverage using a swarm of UAVs in known 3D-terrains, in: Proc. of the International Symposium on Communications, Control and Signal Processing (ISCCSP 2014), Athens, Greece, 2014, pp. 458–461.

[19] M. Torres, D. A. Pelta, J. L. Verdegay, J. C. Torres, Coverage path planning with unmanned aerial vehicles for 3d terrain reconstruction, Expert Systems with Applications 55 (2016) 441–451.

[20] M. Schwager, B. J. Julian, D. Rus, Optimal coverage for multiple hovering robots with downward facing cameras, in: Robotics and Automation, 2009. ICRA'09. IEEE International Conference on, IEEE, Kobe, Japan, 2009, pp. 3515–3522.

[21] M. Schwager, B. J. Julian, M. Angermann, D. Rus, Eyes in the sky: Decentralized control for the deployment of robotic camera networks, Proceedings of the IEEE 99 (9) (2011) 1541–1561.

[22] E. Yanmaz, Connectivity versus area coverage in unmanned aerial vehicle networks, in: Proc. 2012 IEEE International Conference on Communications (ICC), IEEE, Ottawa, Canada, 2012, pp. 719–723.

[23] M. A. Messous, S. M. Senouci, H. Sedjelmaci, Network connectivity and area coverage for UAV fleet mobility model with energy constraint, in: Proc. IEEE Wireless Communications and Networking Conf, 2016, pp. 1–6.

[24] C. Di Franco, G. Buttazzo, Coverage path planning for uavs photogrammetry with energy and resolution constraints, Journal of Intelligent & Robotic Systems (2016) 1–18.

[25] G. S. Avellar, G. A. Pereira, L. C. Pimenta, P. Iscold, Multi-uav routing for area coverage and remote sensing with minimum time, Sensors 15 (11) (2015) 27783–27803.

[26] H. Flanders, Differentiation under the integral sign, American Mathematical Monthly 80 (6) (1973) 615–627.